Electronic Supplementary Information

for

Reversible Open-Close Conformational switching of a Nano-size Metalloporphyrin dimers Triggered by Light and Temperature

Syed Jehanger Shah,[a] Ajitesh Singh,[a] Debabrata Goswami,[a] Masatoshi Ishida[b] and Sankar Prasad Rath*[a]

[a]Department of Chemistry, Indian Institute of Technology Kanpur, Kanpur 208016, India. E-mail: sprath@iitk.ac.in; Fax: +91-512-259-7436; Tel: +91-512-259-7251

[b]Department of Chemistry, Graduate School of Science, Tokyo Metropolitan University, Hachioji, Tokyo 192-0397, Japan.

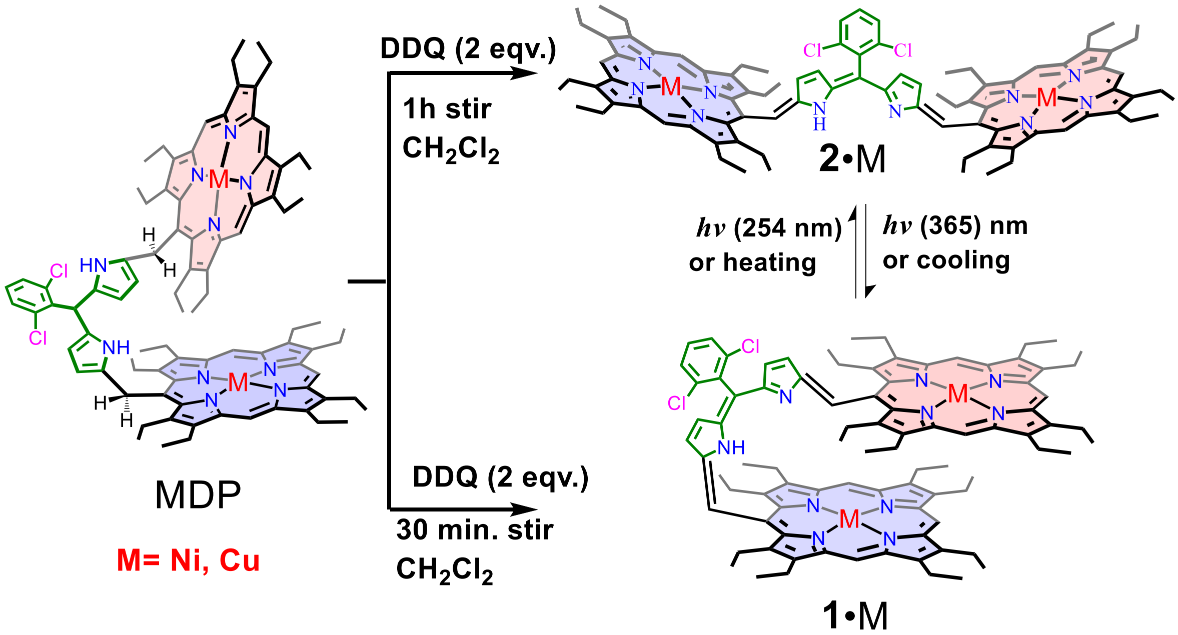

Fig. S1. Synthesis and schematic representation of a reversible open-close conformational switch.

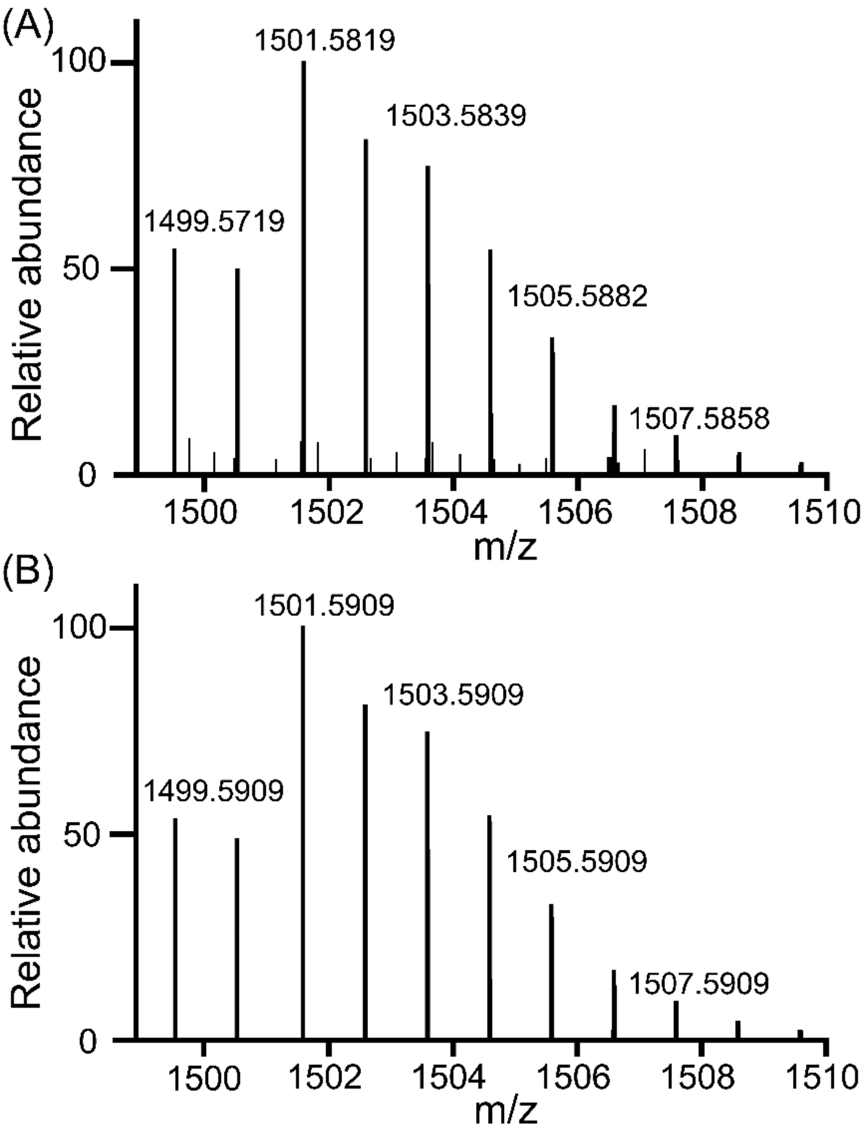

Fig. S2. Isotopic distribution pattern of the (A) experimental and (B) simulated ESI-MS of **1**•Cu.

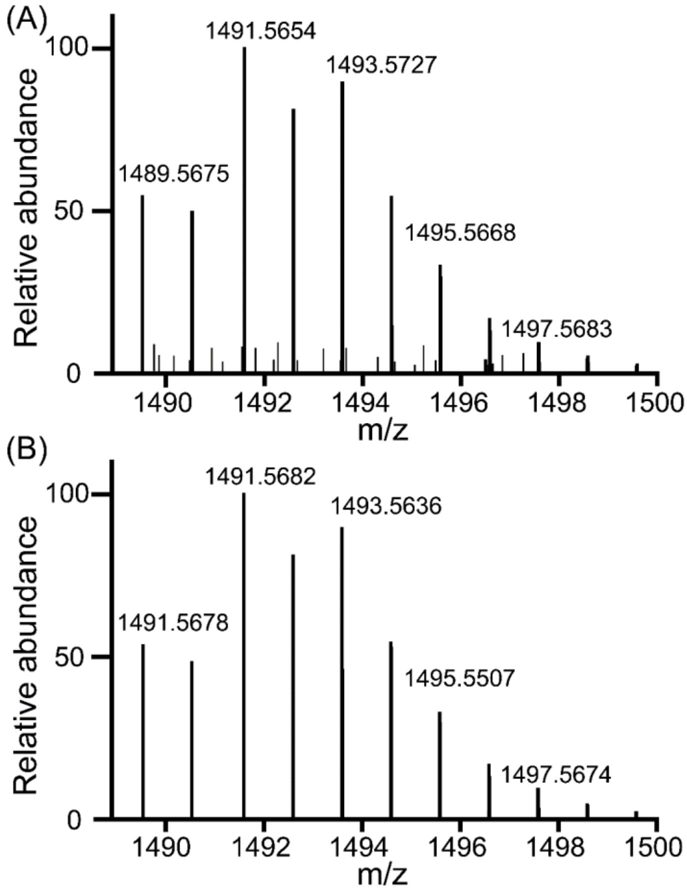

Fig. S3. Isotopic distribution pattern of the (A) experimental and (B) simulated ESI-MS of **1**•Ni.

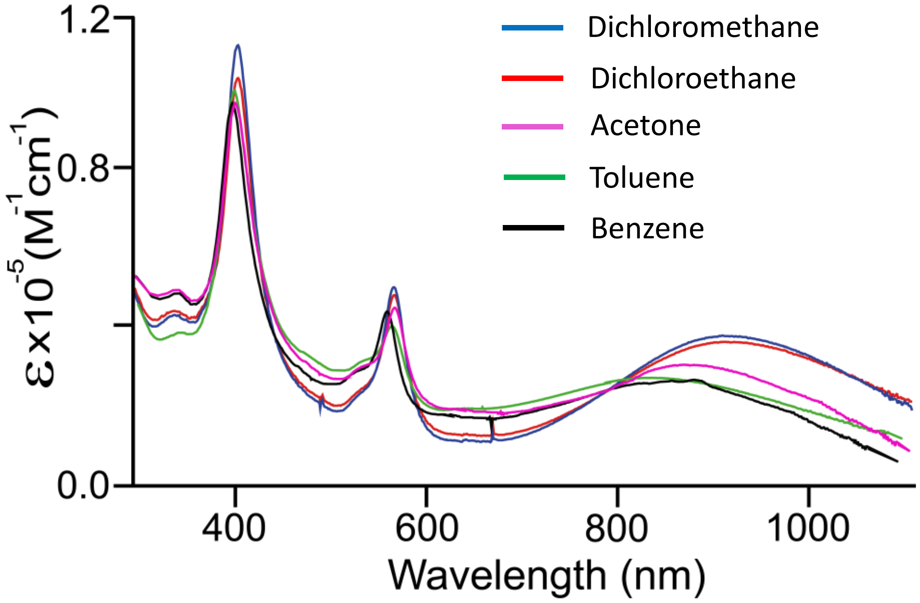

Fig. S4. UV-vis-NIR (at 295 K) solvent dependent spectral changes of **2**•Ni to **1**•Ni in different solvents such as; dichloromethane (blue spectra), dichloroethane (red spectra), acetone (pink spectra), benzene (black spectra), toluene (green spectra).

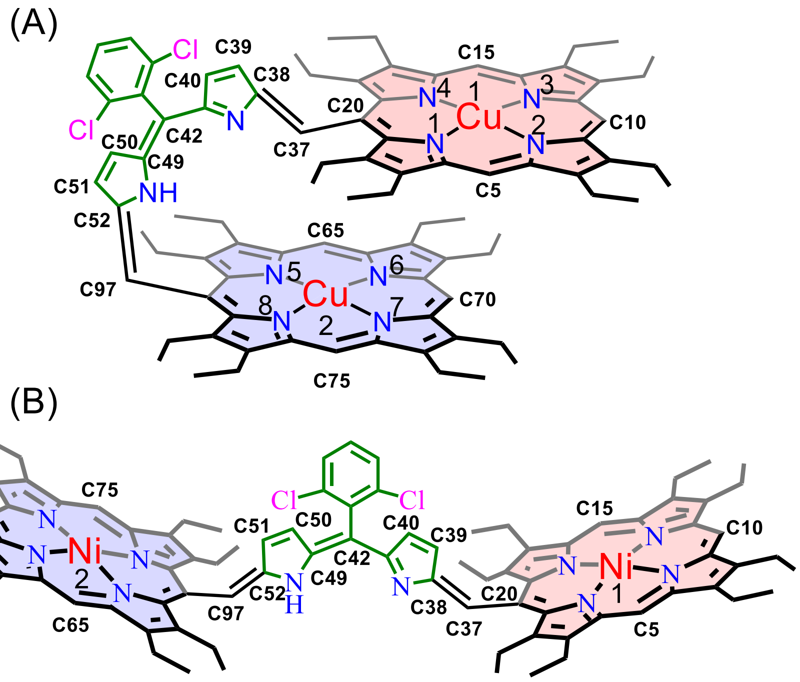

Fig. S5. Atom numbering scheme for (A) **1**•Cu and (B) **2**•Ni

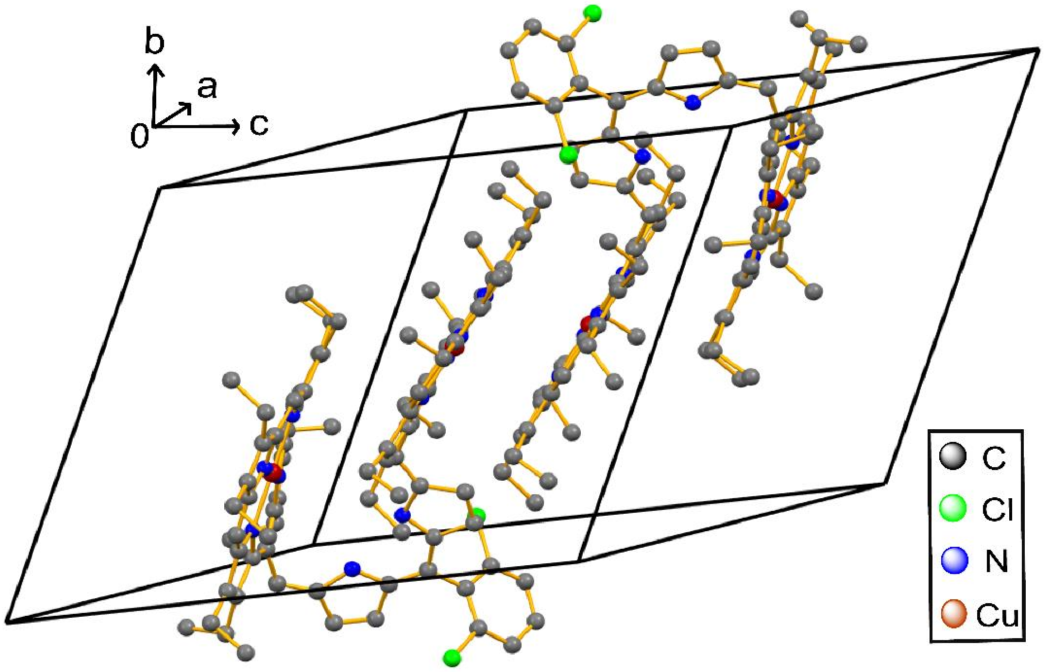

Fig. S6. Diagram showing the molecular packing of **1**•Cu in the unit cell (H atoms have been omitted for clarity).

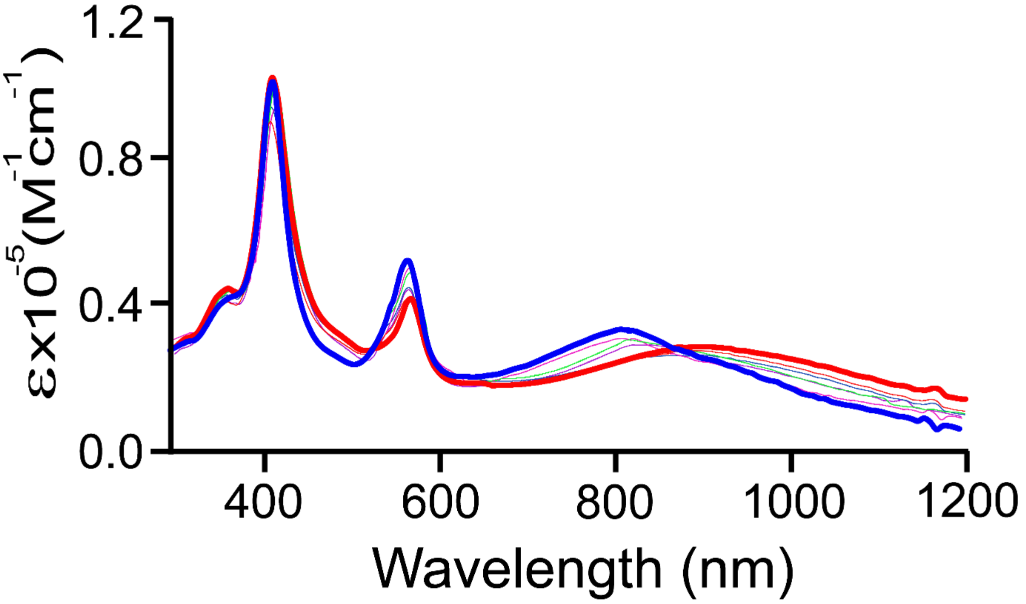

Fig. S7. UV-vis-NIR (in CH_2Cl_2) absorption spectral change upon heating the close form of **1**•Cu (blue line) to give an open form **2**•Cu (red line) and vice-versa on cooling with clear isosbestic points at 532, 615 and 860 nm.

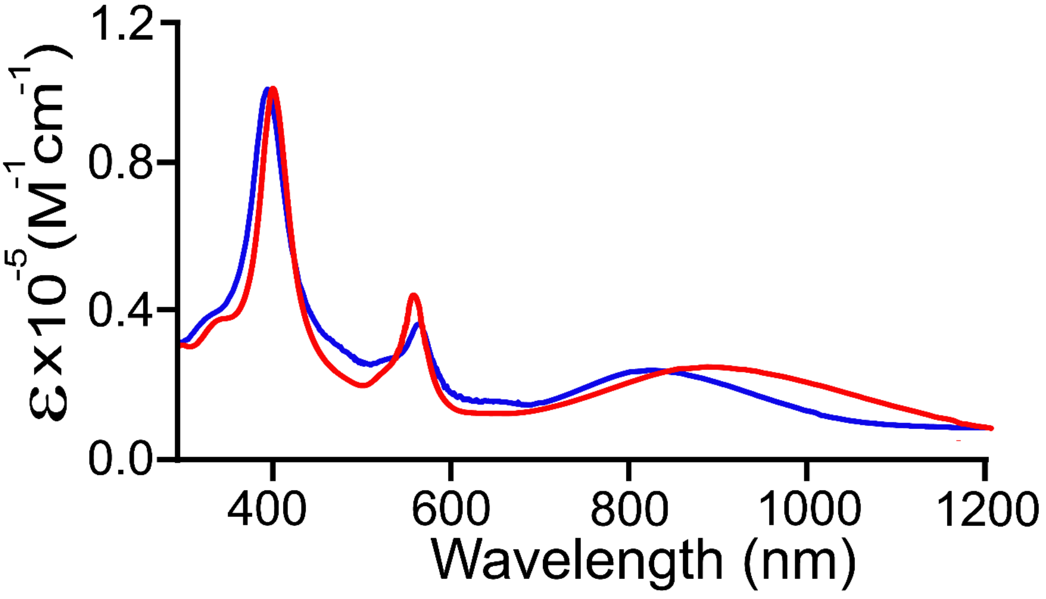

Fig. S8. UV-vis-NIR (in CH_2Cl_2 at 295 K) absorption spectra of **1**•Ni (blue line) and **2**•Ni (red line) interconverted by irradiating with UV-light for 5 minutes at (λ = 254 and 365 nm, respectively).

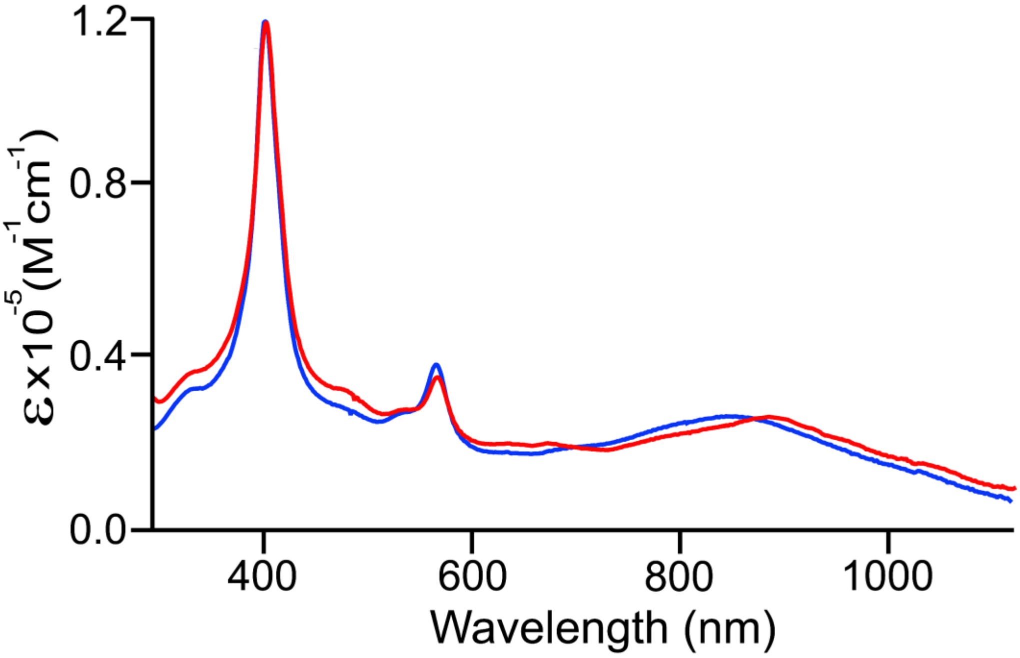

Fig. S9. UV-vis-NIR (in CH_2Cl_2 at 295 K) absorption spectra of **1**•Cu (blue line) and **2**•Cu (red line) interconverted by irradiating with UV-light for 5 minutes at (λ= 254 and 365 nm, respectively).

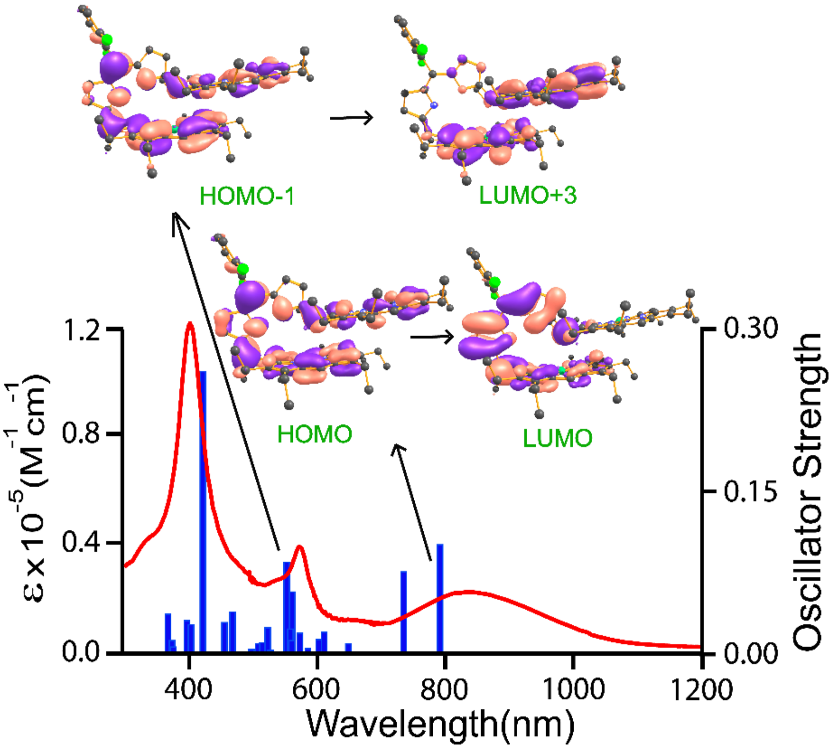

Fig. S10. Electronic absorption spectra (curved line, left axis) in CH_2Cl_2 and oscillator strengths (vertical line, right axis) obtained from TD-DFT calculations at the uB3LYP/6-31G**/LANL2DZ level of theory for **1**•Ni, (The sigma value used in the spectra is 0.1 eV).

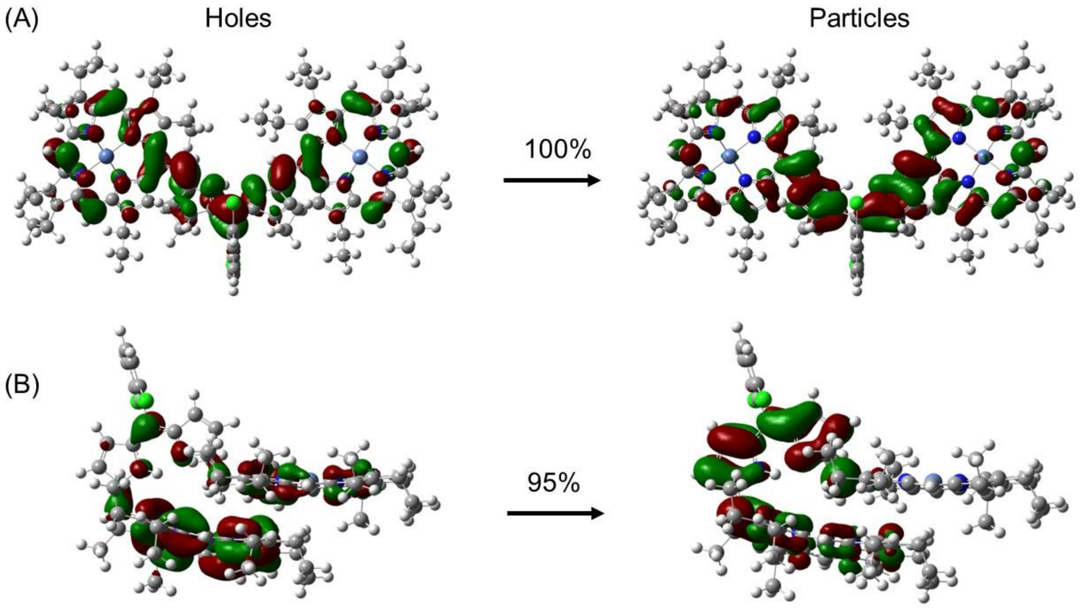

Fig. S11. Natural transition orbitals (NTO) corresponding to the first singlet transitions for (A) **2**•Ni and (B) **1**•Ni obtained by TD-DFT B3LYP/6-31G(d)-LanL2DZ method. Hole refers to the highest occupied natural transition orbital (HONTO), while particle refers to the lowest unoccupied natural transition orbital (LUNTO).

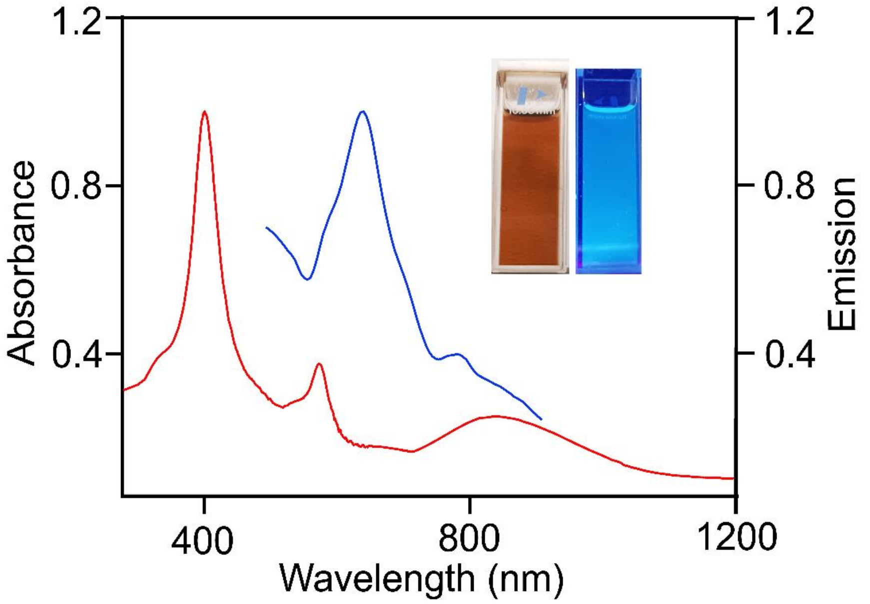

Fig. S12. Normalized absorption (left spectra) of **1**•Ni (red line) and emission (right spectra) (in degassed CH_2Cl_2 at 295 K) of **1**•Ni excited at 560 nm, (light brown under visible light and light blue under UV-light).

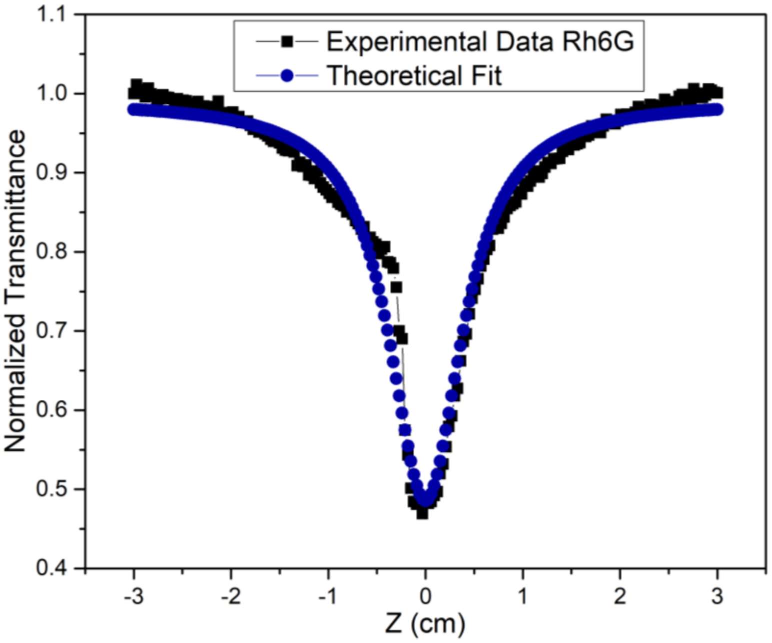

Fig. S13. Open aperture Z-scan data of Rh6G for calibrating the experimental setup with theoretical fit.

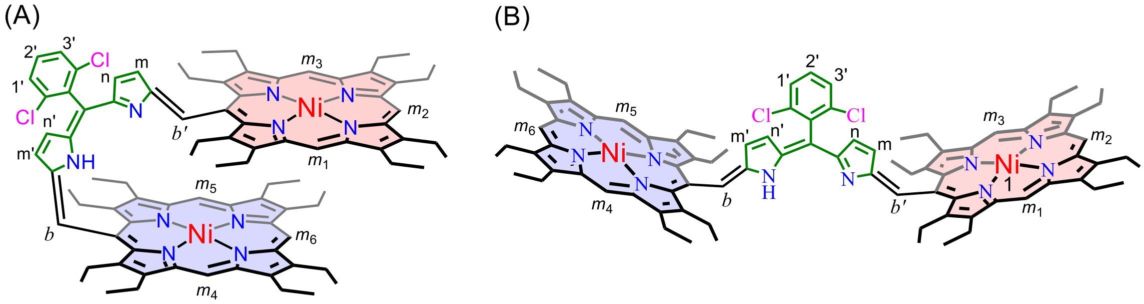

Fig. S14. The numbering scheme used for the ^{1}H NMR assignment for (A) **1**•Ni and (B) **2**•Ni.

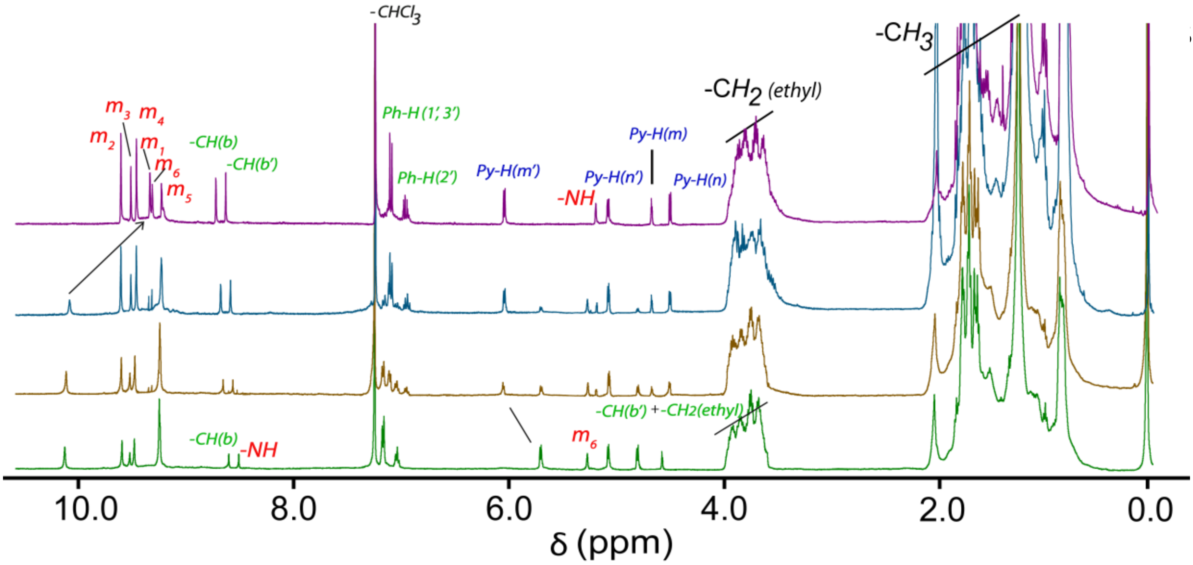

Fig. S15. Stacked ^{1}H NMR spectrum of **1**•Ni determined in CDCl$_3$ at 298 K (green spectra), the second spectra (brown) represent mixture of **1**•Ni and **2**•Ni at 308 K, third spectrum (blue) represent mixture of **1**•Ni and **2**•Ni with increased proportion of **2**•Ni at 318 K and fourth spectra (violet) represents **2**•Ni at 328 K.

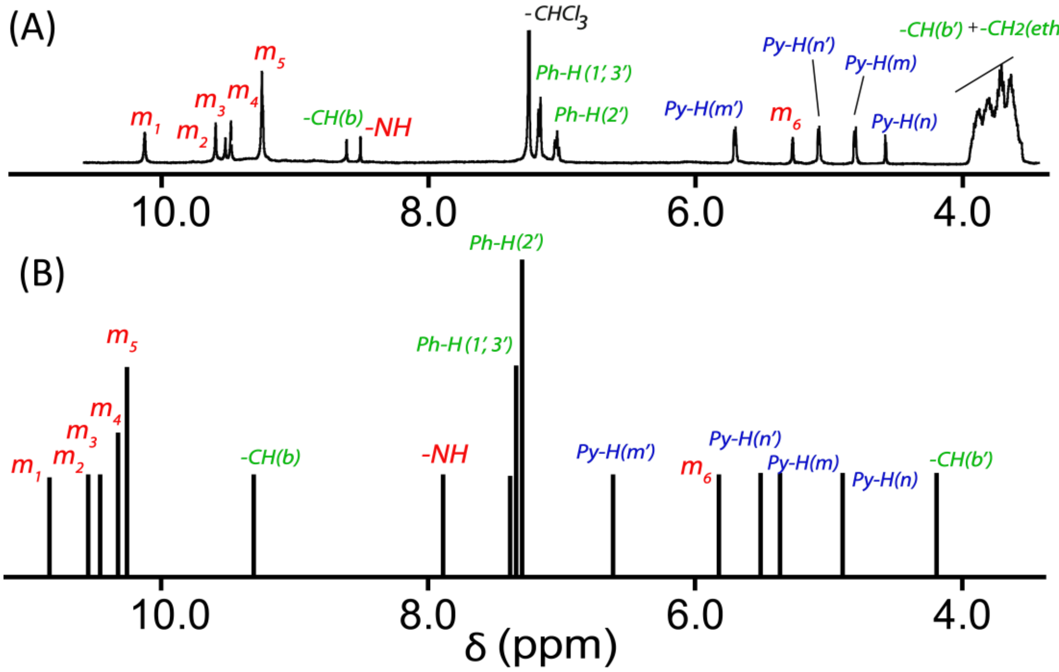

Fig. S16. (A) Experimental ^{1}H NMR (in CDCl$_3$ at 295 K) and (B) calculated ^{1}H NMR spectra of **1**•Ni. Chemical shifts were calculated using uB3LYP/6-31G**/LanL2DZ optimized geometries by GIAO method.

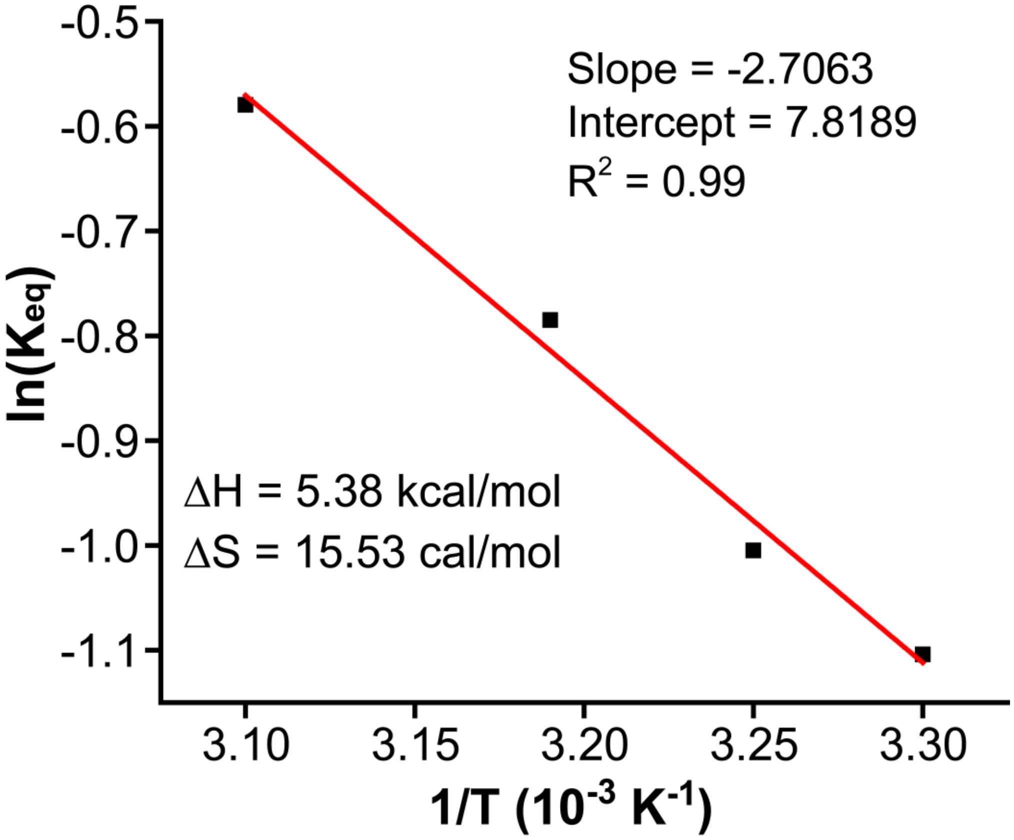

Fig. S17. van't Hoff plot analysis for the conversion of **1**•Ni to **2**•Ni at different temperatures using ^{1}H NMR data. [van't Hoff equation: $\ln(K_{eq}) = -\Delta H/RT + \Delta S/R$, where T = absolute temperature in degrees Kelvin [K], K_{eq} = equilibrium constant; obtained as ratio of [% open]/[% close] at different temperatures (303 K, 308 K, 313 K, and 323 K) , *ΔH* and *ΔS* are the thermodynamic parameters *viz* change in enthalpy and entropy respectively].

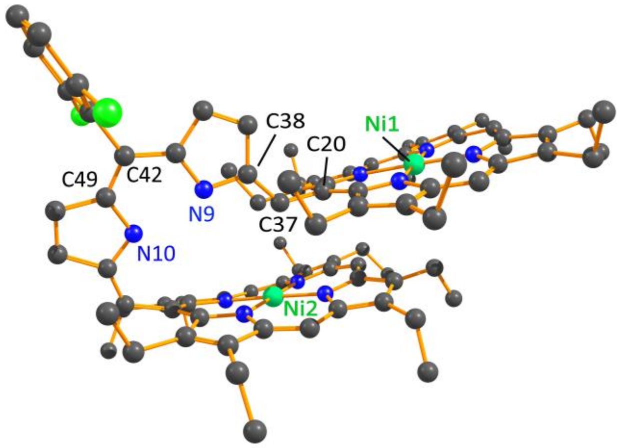

Ni1-N_p	1.981
Ni2-N_p	1.972
C20-C37	1.475
C37-C38	1.351
C42-C49	1.388
C38-N9	1.392
C49-N10	1.367
Θ	15.85

Fig. S18. Optimized geometry of **1**•Ni at the uB3LYP level of theory. Selected bond lengths are given in Å and angle in degree. Parentheses contain the experimental values obtained from the molecular structures of the respective complex.

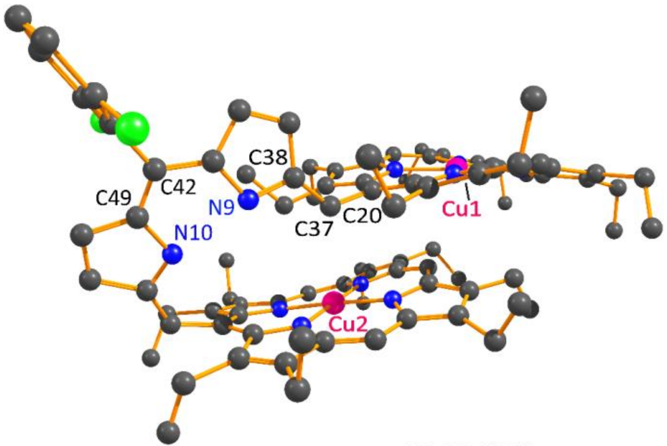

Cu1-N_p	2.018	[2.004(4)]
Cu2-N_p	2.026	[1.996(4)]
C20-C37	1.477	[1.489(7)]
C37-C38	1.352	[1.342(8)]
C42-C49	1.367	[1.363(8)]
C38-N9	1.394	[1.394(9)]
C49-N10	1.367	[1.367(7)]
Θ	8.47	14.22

Fig. S19. Optimized geometry of **1**•Cu at the uB3LYP level of theory. Selected bond lengths are given in Å and angle in degree. Parentheses contain the experimental values obtained from the molecular structures of the respective complex.

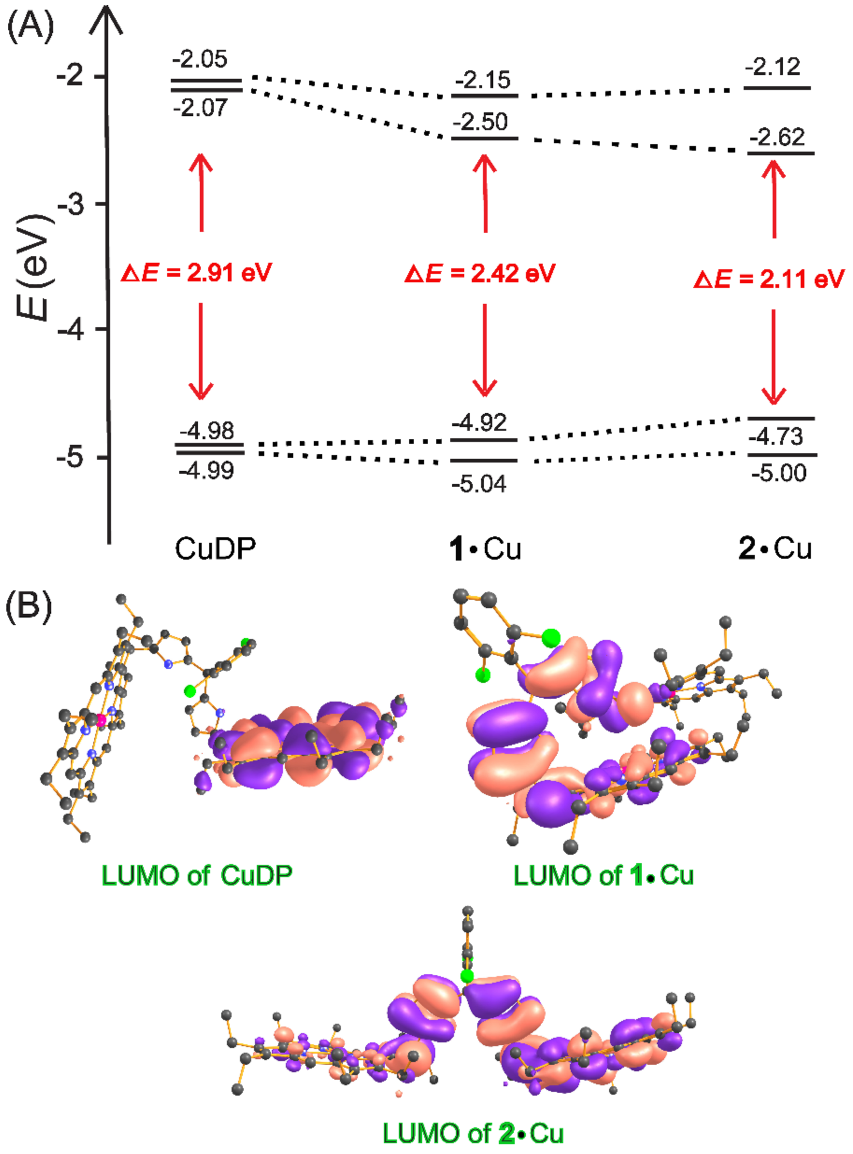

Fig. S20. (A) Energy diagrams of CuDP, **1**•Cu and **2**•Cu (B) Kohn−Sham orbital representations of the LUMOs (isovalue = 0.015).

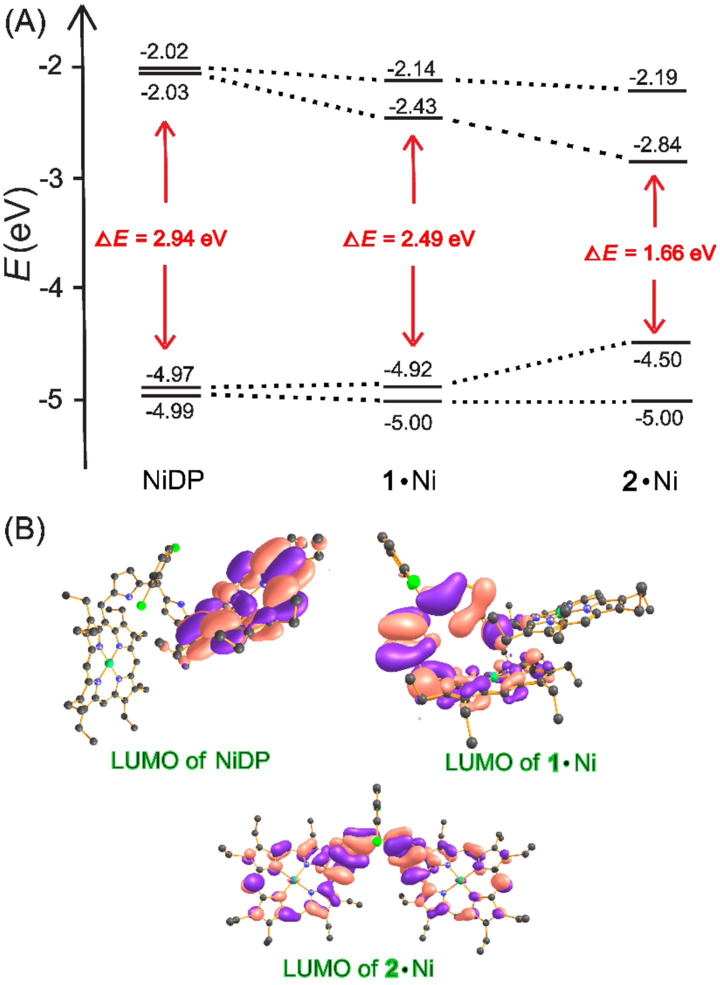

Fig. S21. (A) Energy diagrams of NiDP, **1**•Ni and **2**•Ni (B) Kohn–Sham orbital representations of the LUMOs (isovalue = 0.015).

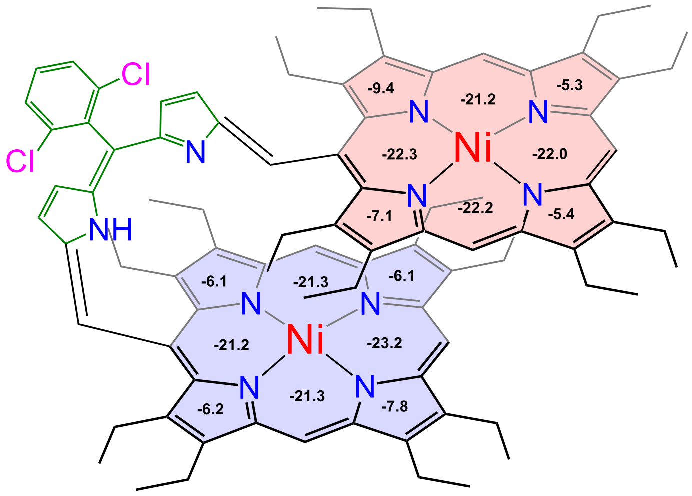

Fig. S22. NICS(0) values of **1**•Ni.

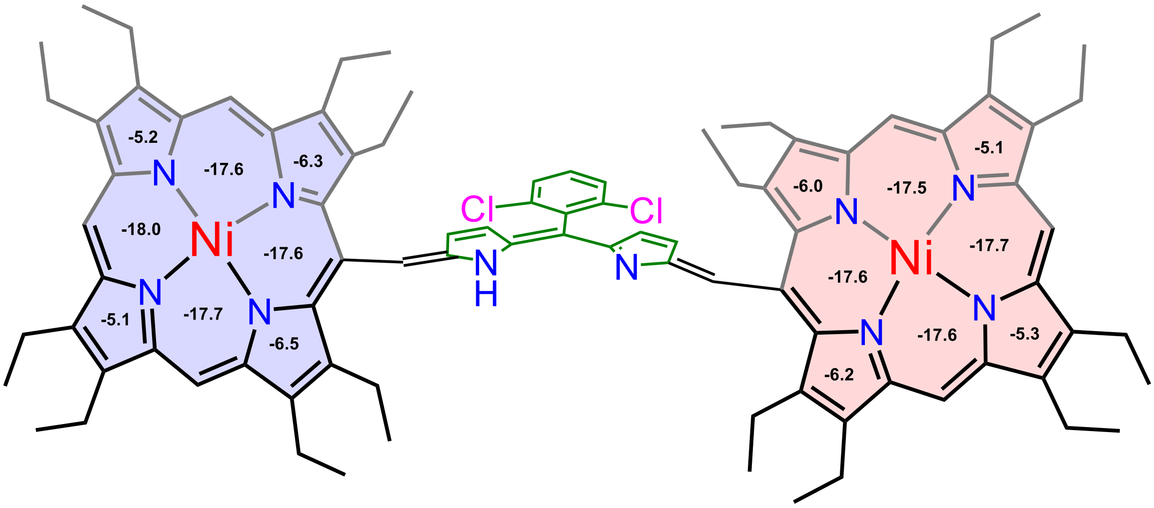

Fig. S23. NICS(0) values of **2**•Ni

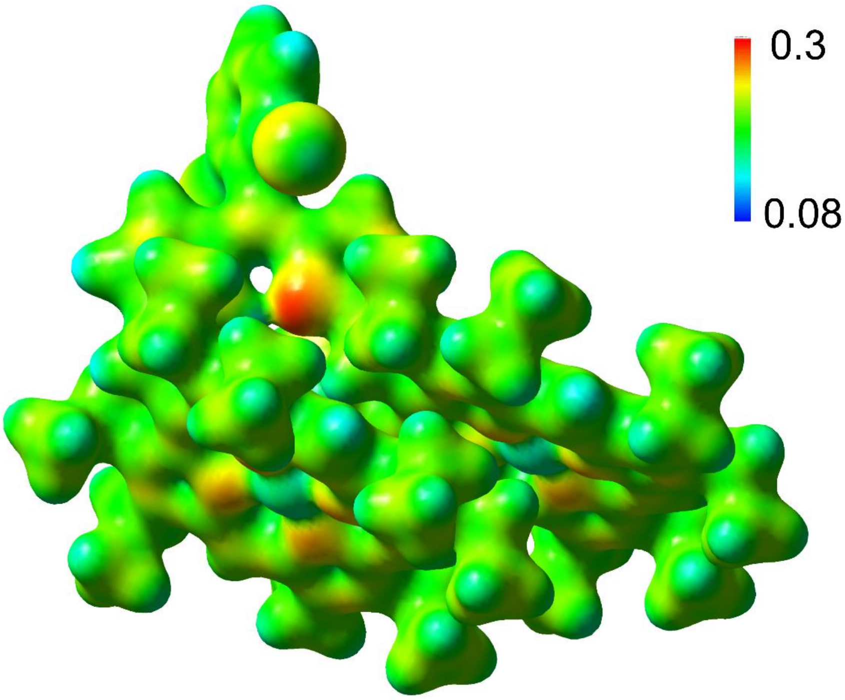

Fig. S24. Electrostatic potential maps of **1**•Ni.

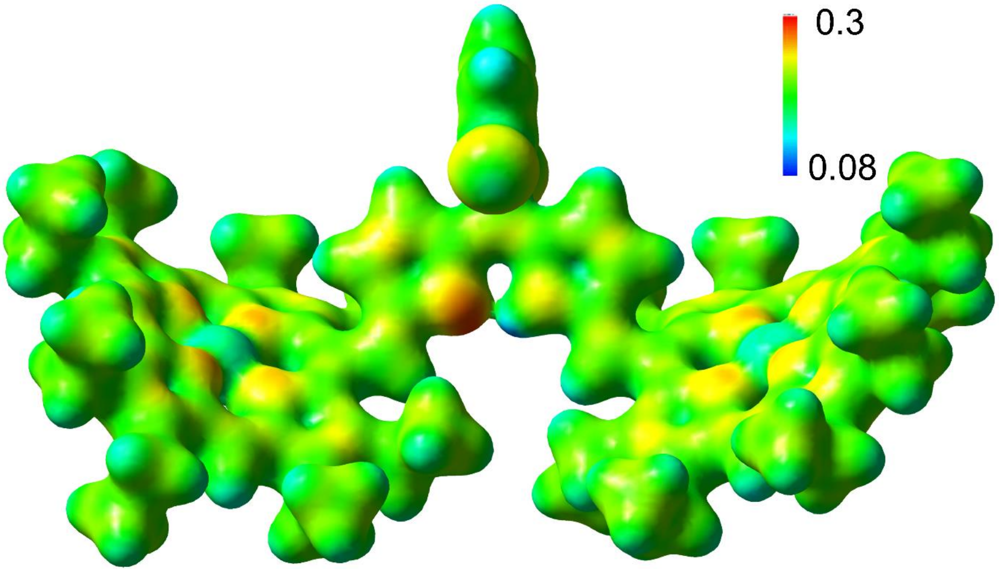

Fig. S25. Electrostatic potential maps of **2**•Ni.

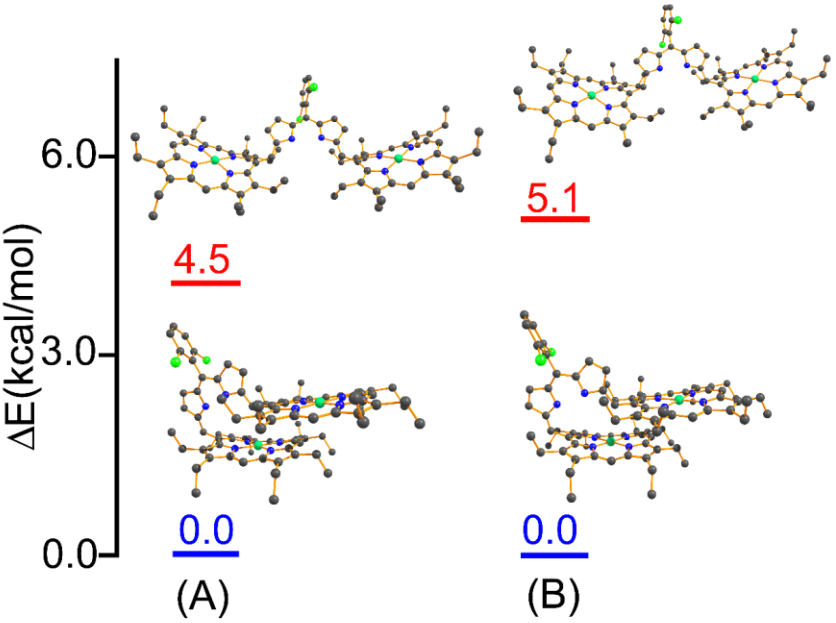

Fig. S26. Relative energies of 'close form' **1**•Ni and 'open form' **2**•Ni as calculated using CAM-B3LYP functional in DFT: (A) gas phase calculation and (B) solvent phase calculation. All energies are relative to close form **1**•Ni.

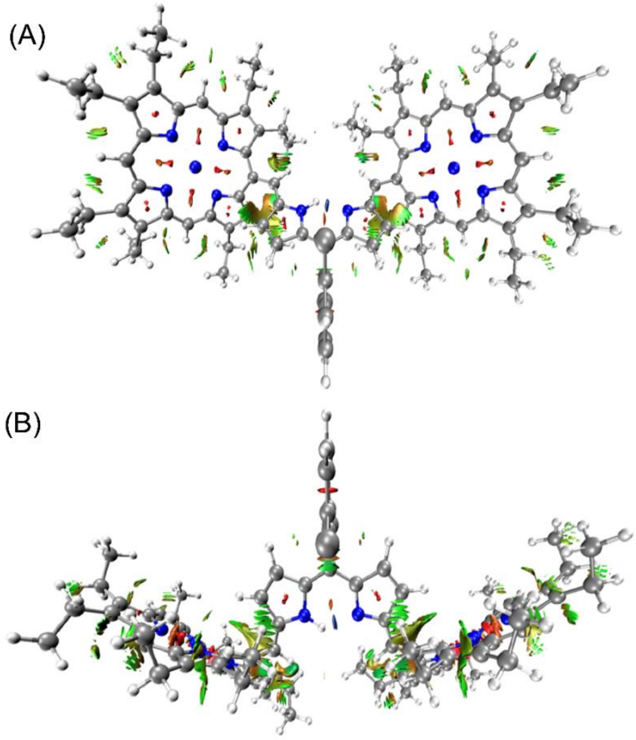

Fig. S27. NCI plots (isosurface value 0.05) of **2**•Cu. (A) front view and (B) side view green isosurface shows regions having noncovalent (van der Waals) interactions. Blue and red isosurfaces show regions having attractive and repulsive interactions, respectively.

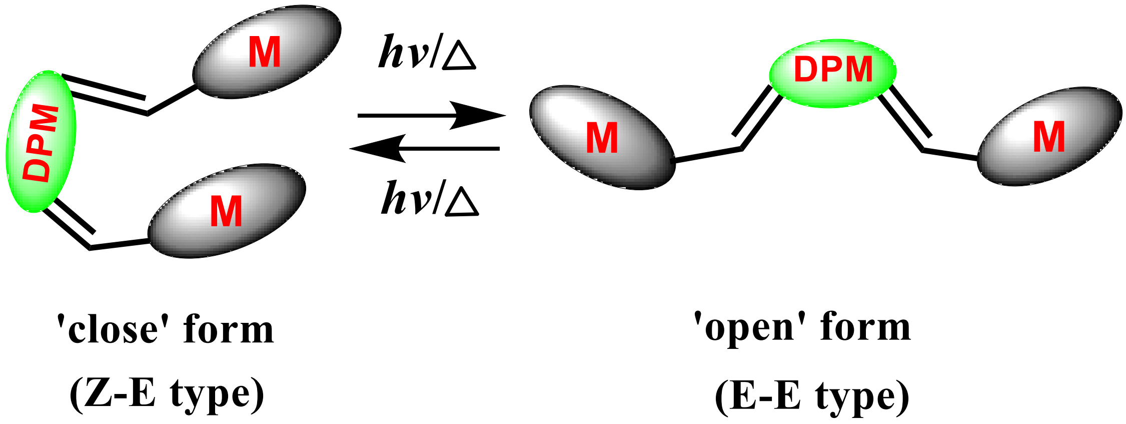

Fig. S28. Scheme depicting nomenclature and geometrical change around double bonds of 'close' form and 'open' form.

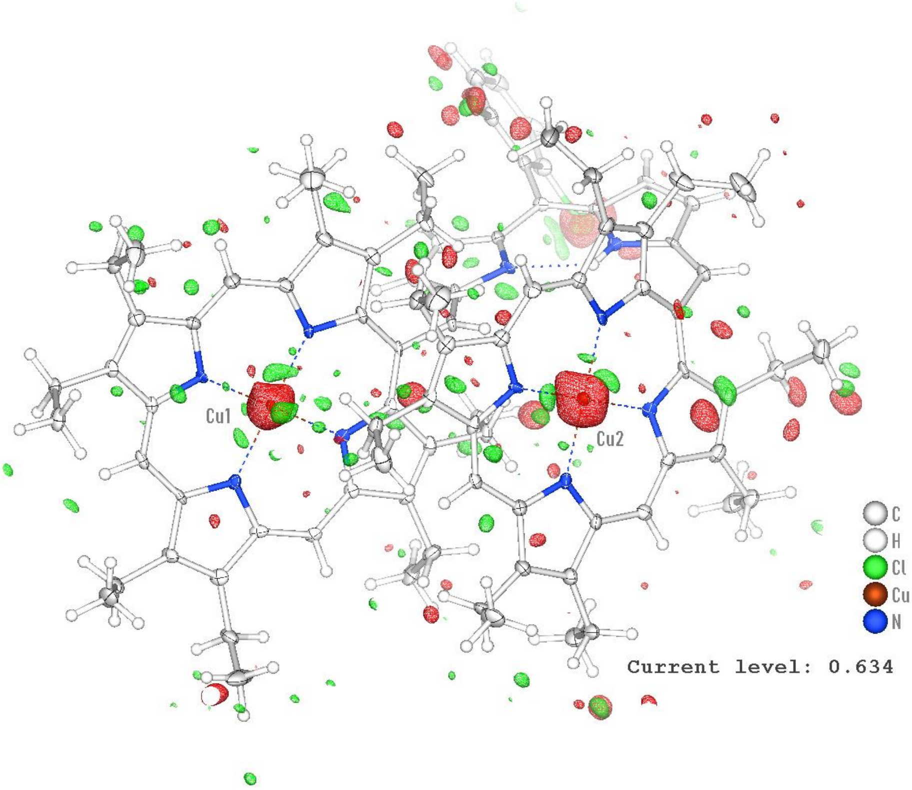

Fig. S29. Diagram showing the residual density plot of the X-ray structure of **1**•Cu.

Table S1. Crystallographic Data and Data Collection Parameters.

	1•Cu
Formula	$C_{89}H_{96}Cl_2Cu_2N_{10}$
T (K)	100(2)
Formula weight	1503.73
Crystal system	Triclinic
Space group	*P-1*
a, Å	15.009(4)
b, Å	15.233(4)
c, Å	20.268(6)
α, deg	69.854(8)
β, deg	74.768(8)
γ, deg	64.853(7)
V, $Å^3$	3900.9(18)
Z	2
dcalcd, g•cm^{-3}	1.280
μ, mm^{-1}	0.666
F(000)	1584
Crystal size, mm^3	0.150 x 0.120 x 0.100
No. of unique data	14516
Completeness to theta = 25.00°	99.9 %
No of parameters refined	944
GOF on F^2	1.153
$R1^a$ [$I > 2\sigma(I)$]	0.0888
$R1^a$ (all data)	0.1147
$wR2^b$ (all data)	0.1804
Largest diff. peak and hole	0.849 and -1.088 e.$Å^{-3}$

$$^{a}R1 = \frac{\Sigma||F_o|-|F_c||}{\Sigma|F_o|}; \quad ^{b}wR2 = \sqrt{\frac{\Sigma\left[w\left(F_o{}^2-F_c{}^2\right)^2\right]}{\Sigma\left[w\left(F_o{}^2\right)^2\right]}}$$